frontiers | Frontiers in Marine Science

TYPE Original Research
PUBLISHED 05 September 2022
DOI 10.3389/fmars.2022.945110

OPEN ACCESS

EDITED BY
Fei Chai,
Ministry of Natural Resources, China

REVIEWED BY
Alexander Matul,
P. P. Shirshov Institute of Oceanology (RAS), Russia
Anne Willem Omta,
Massachusetts Institute of Technology, United States

*CORRESPONDENCE
Longbin Sha
shalongbin@nbu.edu.cn
Yi Zhong
zhongy@sustech.edu.cn

†These authors have contributed equally to this work

SPECIALTY SECTION
This article was submitted to Marine Biogeochemistry, a section of the journal Frontiers in Marine Science

RECEIVED 16 May 2022
ACCEPTED 12 August 2022
PUBLISHED 05 September 2022

CITATION
Liu Y, Qiu Y, Li D, Artemova AV, Zhang Y, Bosin AA, Gorbarenko SA, Liu Q, Zhao D, Sha L and Zhong Y (2022) Abrupt fluctuations in North Pacific Intermediate Water modulated changes in deglacial atmospheric CO_2. *Front. Mar. Sci.* 9:945110. doi: 10.3389/fmars.2022.945110

Abrupt fluctuations in North Pacific Intermediate Water modulated changes in deglacial atmospheric CO_2

Yanguang Liu[1,2†], Yue Qiu[3†], Dongling Li[3], Antonina V. Artemova[4], Yuying Zhang[1,5], Aleksandr A. Bosin[4], Sergey A. Gorbarenko[4], Qingsong Liu[6], Debo Zhao[7], Longbin Sha[3*] and Yi Zhong[6*]

[1]Key Laboratory of Marine Sedimentology and Metallogeny, First Institute of Oceanography, Ministry of Natural Resources (MNR), Qingdao, China, [2]Laboratory for Marine Geology, Pilot National Laboratory for Marine Science and Technology, Qingdao, China, [3]Department of Geography and Spatial Information Techniques, Ningbo University, Ningbo, China, [4]Laboratory of Paleoceanology, V.I. Il'ichev Pacific Oceanological Institute FEB RAS, Vladivostok, Russia, [5]College of Marine Geosciences, Key Laboratory of Submarine Geosciences and Prospecting Technology, Ocean University of China, Qingdao, China, [6]Centre for Marine Magnetism (CM²), Department of Ocean Science and Engineering, Southern University of Science and Technology, Shenzhen, China, [7]Key Laboratory of Marine Geology and Environment, Institute of Oceanology, Chinese Academy of Sciences, Qingdao, China

As a major reservoir of heat and CO_2, the Pacific Ocean is an important component of the global climate system, but the nature of its circulation under different climatic conditions remains poorly understood. We present sedimentary records of surface water hydrography and nutrient dynamics from the subarctic Pacific Ocean, with the aim of investigating changes in sea-ice coverage, biological productivity, and sea surface temperature in the subarctic Northwest Pacific since 32 kyr. Our records indicate an enhanced North Pacific surface water stratification from the last glacial to Heinrich Stadial 1, which generally limited the siliceous productivity supply to the surface water. A productivity peak during the Bølling/Allerød warm interval was associated with an increase in the atmospheric pCO_2, and it was driven by the increased supply of nutrient- and CO_2-rich waters. This process can be attributed to the collapse of the North Pacific Intermediate Water formation at the onset of the Bølling/Allerød interstadial. Moreover, a northward shift of the westerly winds and the gyre boundary could have modulated the expansion of the subpolar gyre, driving changes in poleward heat transport, biogeochemistry, and the hydroclimate of the North Pacific. Our results are consistent with modern evidence for a northward shift of the westerlies in response to global warming, which will likely result in CO_2 outgassing from the subarctic Pacific Ocean in the future.

KEYWORDS

sea surface temperature, North Pacific Intermediate Water, biological productivity, CO_2, subarctic Pacific Ocean

1 Introduction

Deglacial variations in the thermohaline overturning circulation have played a key role in changing atmospheric CO_2 concentrations *via* changes in the upper ocean stratification at high latitudes of the North Pacific and the Southern Ocean (Sigman et al., 2010). In both regions, vertical mixing brings nutrient- and CO_2-rich deep waters into the euphotic zone and facilitates the biological pump, which sequesters atmospheric CO_2 back into the deeper ocean interior (Figure 1A) (Toggweiler, 1999; Honda et al., 2002). Abrupt changes in Southern Ocean stratification occurred during Pleistocene deglaciations, with the reorganizations of circulation and productivity at high latitudes leading to changes in the oceanic oxygen content and a rapid rise in atmospheric CO_2 (Pahnke et al., 2008; Burke and Robinson, 2012; Basak et al., 2018). However, these processes in the North Pacific are poorly understood due to uncertainties regarding its nutrient cycle and the oceanic release of CO_2 *via* deep/intermediate water formation, upwelling, and the associated changes in biogenic productivity (Gray et al., 2018; Praetorius et al., 2020; Rae et al., 2020).

The modern subarctic Pacific Ocean (SPO) is characterized by a steep salinity gradient, with low-salinity surface waters sustained by a large freshwater influx and relatively low regional evaporation (Figure 1B; Warren, 1983; Broecker, 1990; Emile-Geay et al., 2003). Several modeling studies have shown that perturbations in the surface ocean in the North Pacific can substantially impact the Northern Hemisphere climate *via* changes in the sea-ice extent and poleward moisture transport (Praetorius et al., 2018). Several studies have suggested that North Pacific Intermediate Water (NPIW) formation increased during glacial and stadial conditions (Matsumoto et al., 2002; Herguera et al., 2010; Okazaki et al., 2010), and therefore the North Pacific deep water has been regarded as an efficient glacial CO_2 store (Galbraith et al., 2007). Although there is an increasing amount of evidence for deglacial upwelling that may have led to enhanced biological productivity during the Bølling/Allerød interstadial (B/A; Galbraith et al., 2007; Kohfeld and Chase, 2011), it remains controversial how deep convective overturning processes influence the entire atmospheric CO_2 store and its release.

Past changes in deep convective overturning can be reconstructed from records of sea-ice cover, surface temperature, and biological productivity (Gray et al., 2018). Since diatoms are the main component of phytoplankton in this region, high diatom productivity results in pulses of opal flux that are indicators of marine productivity variations (Honjo, 1984; Takahashi, 1986). Diatom assemblages are also sensitive to changes in water mass, sea-ice conditions, and biological productivity (Ren et al., 2014). Therefore, we obtained records of diatom assemblages and biogenic opal and sea surface temperature (SST) from the SPO, at a millennial-scale resolution, during the Last Glacial Maximum (LGM) and the interval following the last deglaciation. Our main objective was to investigate changes in sea-ice coverage, biological productivity, and SST in the SPO, and to determine the driving mechanisms. Our findings potentially improve our understanding of deglacial circulation in the North Pacific and its role in changing atmospheric CO_2.

2 Oceanographic setting

The SPO has an extremely complex pattern of past climate change, and it plays an important role in Earth's oceanic and climatic evolution (Davis et al., 2020). It is linked with the Sea of Okhotsk in the west *via* the many straits of the Kuril Islands, and the Bering Sea in the north *via* the straits of the Aleutian Islands. The subarctic Northwest (NW) Pacific is a eutrophic environment, with a shallow (15–25 m) euphotic zone (Venrick, 1991). Core LV63-4-2 was collected from the Detroit Seamount, which lies at the northernmost end of the Hawaiian-Emperor Seamount Chain (Figure 1).

The surface circulation in the North Pacific Ocean, including the Subarctic Gyre (Dodimead et al., 1963) and the Subtropical Gyre, regulates the exchange of heat and nutrients between different ocean regions (Qiu, 2002). The Subarctic Gyre, bounded by the high surface temperature gradient of the Subarctic Front in the south, consists of two counterclockwise circulating systems: the Alaskan Gyre (AG) in the east and the Western Subarctic Gyre (WSG) in the west (Figure 1B). The WSG is located at the confluence of the Bering Sea, the Sea of Okhotsk, and the North Pacific Ocean, and it exhibits varying characteristics, depending on the relative dominance of these water types (Sancetta, 1979). The Alaskan Stream (AS) forms the northern boundary current and transports water masses from the AG along the Aleutian Islands into the western subpolar gyre, which then enter the Bering Sea through several passages between the Aleutian Islands. There are upwelling domains in the easternmost and westernmost areas of the western subarctic Pacific. The water mass associated with the easternmost upwelling is advected to the west by the effect of the AS, which flows westward. This upwelled water mass thus reaches the euphotic layer above the Emperor Seamount Chain (Venrick, 1991).

As a consequence of the halocline, no deep water is formed in the modern subarctic Pacific realm. Intermediate water formation is restricted to the marginal Sea of Okhotsk, from where well-ventilated Okhotsk Sea Intermediate Water, produced in coastal polynyas by brine rejection during sea-ice formation in winter (Shcherbina et al., 2003), exits *via* the Kurile Straits, mixes with waters from the WSG (Yasuda, 1997; You, 2003), and further south with Kuroshio waters, thereby forming NPIW. Due to these ocean current systems, the western North Pacific has a steeper temperature gradient than the eastern North

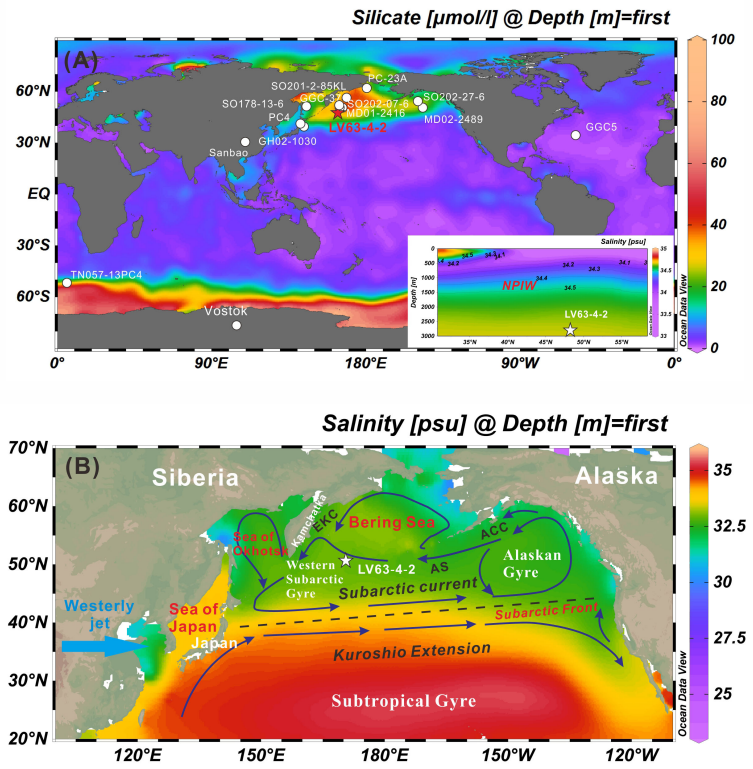

FIGURE 1
Locations of the cores that were referred to in this paper and the modern regional settings in the study area. **(A)** Global map of the mean annual silicic acid concentration. The sediment cores are from the following locations: (i) the subarctic Pacific Ocean LV63-4-2 (this study), GGC-37 (Lam et al., 2013), MD01-2416 (Gebhardt et al., 2008), SO202-27-6 (Maier et al., 2015), and MD02-2489 (Rae et al., 2014); (ii) the Bering Sea SO201-2-85KL (Max et al., 2014) and PC-23A (Rella et al., 2012); (iii) the Sea of Okhotsk SO178-13-6 and PC4 (Hoshiba et al., 2006); and (iv) other GH02-1030 (Okazaki et al., 2010), GGC05 (McManus et al., 2004), and TN057-13PC4 (Anderson et al., 2009). Map of the salinity distribution of intermediate water in the North Pacific in the right corner**(B)** Mean annual sea surface salinity (Antonov et al., 2010) and ocean surface currents (after Dodimead et al., 1963; Stabeno et al., 2004); abbreviations: ACC, Alaska Coastal Current; AS, Alaskan Stream; EKC, East Kamchatka Current. The maps were created using Ocean Data View (www.odv.awi.de).

Pacific. High concentrations of macronutrients (nitrate, phosphate, and silicate), iron, and chlorophyll are recorded in the western North Pacific, while no substantial differences are found between the primary productivity in the western and eastern North Pacific (Ren et al., 2014).

In the high-latitude areas of the North Pacific, the light limitation allows for nutrient concentrations to build up over winter (Harrison et al., 1999), and iron limitation results in year-round high nitrate but low chlorophyll concentrations in the surface water (HNLC) (Martin and Fitzwater, 1988). The abundant nutrients in SPO regions are partially utilized during spring blooms, with diatom productivity dominating the large phytoplankton community. In spring, there is an outbreak of siliceous (diatom) phytoplankton and this spring peak in productivity extends from April to July, thus capturing the beginning of summer (Honjo and Doherty, 1988; Okazaki et al., 2005). Phytoplankton blooming continues in summer due to the active vertical mixing of water in local eddies and upwellings and enhanced remineralization within the upper active highly-stratified layer. The bulk of this material is supplied during relatively short periods: more than 50% of the annual runoff of diatoms was recorded from May to June. In autumn, a less pronounced productivity peak is caused by the development of calcareous microorganisms (coccolithophorids during August to September), siliceous protozoa (radiolarians during March to June), and, to a lesser extent, diatoms (Tanimura, 1992; Tsoy and Wong, 1999; Onodera and Takahashi, 2005). The lowest diatom productivity was recorded between November and February.

3 Material and methods

3.1 Core locations and stratigraphy

Gravity core LV63-4-2 (51.63°N, 167.81°E; 2,946 m water depth) was recovered during the joint Russian-Chinese cruise 63 of the R/V "*Akademik M.A. Lavrentyev*" in 2013. The core

TABLE 1 Age model for the upper part (0-190 cm) of core LV63-4-2 according to AMS ^{14}C data of Zhong et al. (2020).

Depth (cm)	conventional age (yr)	Age Error (yr)	Calibrated Age (cal yr BP)	Tie-point	Linear Sediment Rate (cm/kyr)
11-13	6030	30	5919	AMS^{14}C	2.03
31-33	10080	40	10435	AMS^{14}C	4.43
40	—	—	12800	L^*, δ^{18}O	3.38
53-55	12690	50	13640	AMS^{14}C	16.7
60	—	—	14692	δ^{18}O	5.99
98-100	14690	50	16670	AMS^{14}C	19.16
108-110	16130	60	18490	AMS^{14}C	5.5
149-151	18950	70	21860	AMS^{14}C	12.2
190	—	—	28900	L^*, δ^{18}O	5.68

site is on the Detroit Seamount in an area influenced by the WSG (Figure 1). The sediment lithology is relatively uniform, mainly consisting of gray to grayish-green mud. Age models for the deglacial part of the core are provided by Zhong et al. (2020). Accelerator mass spectrometry ^{14}C ages were measured based on the planktonic foraminifer *Neogloboquadrina pachyderma* (Ehrenberg; sinistral) by Beta Analytic Inc., USA. Calendar age conversions were performed using Marine13 with *Calib 7.0.2* software (Reimer et al., 2013). All the measured ^{14}C ages were then corrected for a sea surface water reservoir age ($\triangle$R) of 500 years (Table 1). The stratigraphic framework of the entire core was obtained by linear interpolation between the ^{14}C ages. The uncertainty of the age model was reasonably constant and relatively small throughout the core. The studied interval of core LV63-4-2 is 203-cm long, comprising the last glacial-deglacial-Holocene interval (the last ~32 kyr).

3.2 Diatom analysis

A total of 67 diatom samples were collected from the uppermost 203 cm of core LV63-4-2. Diatom samples were taken every 2–4 cm and prepared using standard methods. The diatom concentration per 1 g of dry sediment was then determined, together with the species compositions (Jousé, 1962). Diatom identification and counting were conducted using a Mikmed-6 microscope (LOMO, Russia) at ×900 and ×1300 magnifications, and 300–350 frustules were identified for each slide. To determine the diatom concentration, the number of frustules in several horizontal traverses was counted and recalculated as the absolute number per 1 g of sediment. Thereafter, we used a heavy potassium-cadmium liquid containing cadmium iodide (CdI_2) and potassium iodide (KI) in the following ratio H_2O:CdI_2:KI = 1:2.5:2.25 to extract the frustules from the diatom-depleted sediment. Diatom assemblage analysis was conducted at the V. I. Il'ichev Pacific Oceanological Institute, Far East Branch of the Russian Academy of Sciences, Russia.

3.3 Glycerol dialkyl glycerol tetraethers lipids

Analyses of glycerol dialkyl glycerol tetraethers (GDGTs), membrane lipids of archaea and certain bacteria, can be used to determine the organic matter source, microbial community, and paleo-temperature and pH (Schouten et al., 2013). The 68 sediment samples (~5 g) were freeze-dried and homogenized and then 10 μg of C46-GDGT was added as an internal standard. The samples were then extracted using an accelerated solvent extractor (Dionex ASE200, Thermo Scientific^{TM}, USA) with 22 mL cells and dichloromethane (DCM). Methanol (MeOH) 2:1 (vol/vol) was used as the solvent and the extraction was conducted at 100°C and 6.895×10^6 Pa, with three cycles of 5 min each. The total lipid extracts were dried using a rotary evaporator. The samples were then hydrolyzed with 0.1 N potassium hydroxide (KOH) in MeOH:H_2O 9:1 (vol/vol). Neutral compounds (including GDGTs) were extracted with n-hexane. Thereafter, different compound classes were separated using column chromatography and deactivated silicon dioxide (SiO_2). The polar fraction was eluted using n-hexane. Polar compound classes, including GDGTs, were eluted with MeOH : DCM 1:1 (vol/vol). After dissolution in hexane:isopropanol 99:1 (vol/vol) the polar fraction was filtered using a polytetrafluoroethylene filter (0.45 μm pore size) according to the methods of Hopmans et al. (2004). The samples were then brought to a concentration of 2 μg/μL prior to the GDGTs analysis.

GDGTs were analyzed using high-performance liquid chromatography coupled *via* an atmospheric pressure chemical ionization interface to a single quadrupole mass selective detector, following the methods of Chen et al. (2014). The mass selective detector was set for selected ion monitoring of the following $[M + H]^+$ ions: *m/z* 1302.3 (GDGT-0), 1300.3 (GDGT-1), 1298.3 (GDGT-2), 1296.3 (GDGT-3), and 1292.3 (GDGT-4+4′/crenarcheol + regio-isomer). Kim et al. (2010) suggested that TEX_{86}^L, one of the modified versions of TEX_{86}, has the best correlation with annual mean surface temperatures within the range of -3°C to 30°C and is applicable of temperature

reconstruction in the subpolar ocean. It is defined as:

$$TEX_{86}^{L} = Log\left\{\frac{[GDGT-2]}{[GDGT-1]+[GDGT-2]+[GDGT-3]}\right\} \quad (1)$$

where the structure of GDGT-1, GDGT-2, and GDGT-3 are given in Schouten et al. (2002).

To convert TEX_{86}^{L} to temperature, we applied the regional calibration for the Sea of Okhotsk and the NW Pacific of Seki et al. (2004). The calibration equation is as follows:

$$SST_{L} = 27.2 \times TEX_{86}^{L} + 21.8 \quad (2)$$

In most areas of the modern ocean, Thaumarchaeota, as the primary GDGTs producers in archaea, reach their maximum abundance near the base of the euphotic zone or in the epipelagic zone (50–200 m), and decrease towards the mesopelagic zone (Mincer et al., 2007; Church et al., 2010; Dong et al., 2015). As a result, TEX_{86}^{L} can be used as a temperature proxy for near-surface to shallow subsurface (< 200 m) waters (Zhang and Liu, 2018).

4 Results

4.1 Diatoms as paleoenvironmental indicators

Diatoms are widespread in marine environments and are highly sensitive to the environmental conditions. Changes in diatom abundance and species composition in marine sediments can often be used for palaeoenvironmental reconstruction. Sixty species of diatoms were identified in the sediment of core LV63-4-2, mainly marine planktonic species, but a few freshwater species were sporadically identified, including *Pinnularia borealis* Ehrenberg, *Grammatophora oceanica* Ehrenberg, and *Fragilaria* spp. The relative abundance (%) of the most important diatom species, with specific environmental significance, are illustrated in Figure 2.

The marine diatoms in core LV63-4-2 can be divided into several ecological groups, which are indicative of paleoceanographic conditions, including open-oceanic cold-water species, sea-ice related species, benthic species, and warm-water species. The ecological groups and their environmental significance are as follows:

Open-oceanic cold-water species: *Rhizosolenia hebetata* var. *hiemalis* Gran, *Shionodiscus latimarginatus* Makarova, *Thalassiothrix longissima* Cleve and Grunow, the *Actinocyclus* group (*Actinocyclus curvatulus* Janisch, *Actinocyclus ochotensis* Jousé, and *Actinocyclus divisus* Grunow), and *Coscinodiscus marginatus* Ehrenberg. Open-oceanic cold-water species comprised up to 98% of the total diatom and were dominant in the study area during the last 32 kyr, except for the interval of 14.5–11.5 kyr BP (Figure 2).

Sea-ice related species: *Fragilariopsis cylindrus* (Grunow) Krieger in Helmcke and Krieger, *Fragilariopsis oceanica* (Cleve) Hasle, and *Fossula arctica* Hasle, Syversten and Von Quillfeldt. These diatoms vegetate both on and beneath the ice and are considered reliable tools for reconstructing the coverage or drifting of sea-ice (Horner and Alexander, 1972). Hasle and Heimdal (1968) reported that *Thalassiosira gravida* Cleve (=*Thalassiosira antarctica* Comber) is restricted to coastal or ice-margin waters under conditions of low temperature (-1–4°C) and salinity (25–34‰). However, a map of the relative

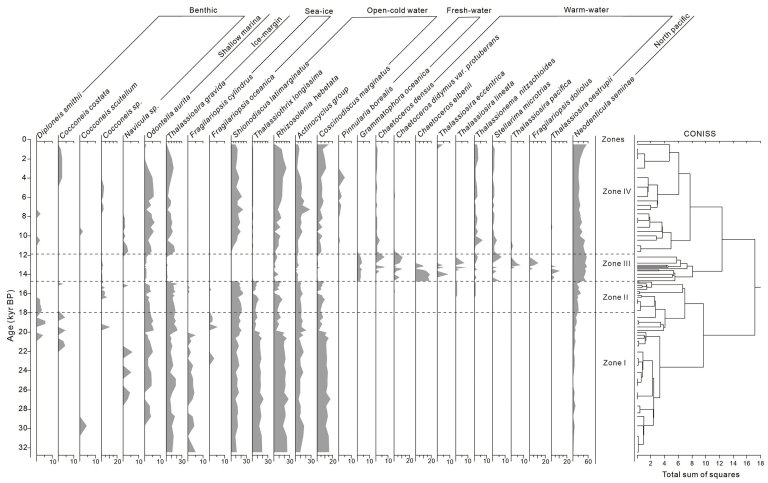

FIGURE 2
Relative abundance (%) of selected paleoenvironmental indicators in the diatom assemblages of core LV63-4-2. According to the results of stratigraphically-constrained cluster analysis, the diatom assemblages of core LV63-4-2 over the past 32 kyr can be divided into four zones (Zones I–IV). The plot was created using *Tilia* software.

abundance of diatom species in the surface sediments of the North Pacific suggests a more complicated ecology for *T. gravida*, and its highest abundances occur on the Bering Shelf, along the Kamchatka Peninsula, and off the Kuril Islands (Ren et al., 2014). Other studies have shown that *T. gravida* resting spores are confined to cold-water neritic areas (on the continental shelf and slope), and it is also abundant among early spring phytoplankton communities, both within and beyond areas of seasonal sea-ice (Poulin et al., 2010; Thomas et al., 2018). Also, several researchers have proposed that the abundance of *T. gravida* is positively correlated with the sea-ice concentration (Koc Karpuz and Schrader, 1990; Shiga and Koizumi, 1999). Since it is a bipolar species, it is widely distributed among the Antarctic and Arctic plankton; however, it is rarely observed in the Antarctic, since it lives within the ice and is therefore more often observed within the under-ice plankton and in the surface water layer (Gogorev, 2013). Okada (2002) used the relative abundance of this species as an index of the amount of sea-ice at observation sites in the western subarctic Pacific. Therefore, *T. gravida* was included as an ice-margin species in this study.

Benthic species: *Diploneis smithii* (Brébisson) Cleve, *Actinoptychus senarius* (Ehrenberg) Ehrenberg, *Cocconeis costata* Gregory, and *Cocconeis scutellum* Ehrenberg.

Warm-water (subtropical to temperate water) species: *Thalassiosira eccentrica* (Ehrenberg) Cleve, *Thalassiosira lineata* Jousé, *Thalassionema nitzschioides* (Grunow) Mereschkowsky, *Azpeitia nodulifer* (Schmidt) Fryxell and Sims, *Thalassiosira pacifica* Gran and Angst, *Fragilariopsis doliolus* (Wallich) Medlin and Sims, and *Thalassiosira oestrupii* (Ostenfeld) Hasle. These species are recognized as warm-water oceanic taxa and are distributed in the subtropical and temperate waters of the North Pacific Ocean (Sancetta and Calvert, 1988; Sancetta, 1992; Tanimura, 1992; Crosta et al., 2005; Onodera and Takahashi, 2005).

Neodenticula seminae (Simonsen and Kanaya) Akiba and Yanagisaw, the most dominant species in core LV63-4-2, is an endemic planktonic diatom species of subarctic Pacific waters, which have moderate summer SSTs and relatively high salinity (Onodera and Takahashi, 2005). A high abundance (> 10%) of this species has been recorded in surface sediment samples from areas with temperatures between 8 and 15°C (Sancetta, 1982; Ren et al., 2014; Sattarova and Artemova, 2015). Previous studies found that this species is abundant in the northernmost NW Pacific, Bering Sea Basin, Gulf of Alaska, and along the Aleutian Islands, but it is rare in the shallow continental shelf area and the Chukchi Sea at higher latitudes. It is also rarely found south of 42°N (Ren et al., 2014). Additionally, surface sediment samples, collected along the Aleutian Current, from the Gulf of Alaska to the Bowers Ridge, contained > 50% *N. seminae* (Ren et al., 2014). This species, therefore, is regarded as a tracer for the Aleutian Current and a decrease in its abundance suggests a reduction in the inflow of AS water (Teraishi et al., 2016; Stroynowski et al., 2017). *N. seminae* is also characteristic of high nutrient concentrations and was dominant during interglacial periods when it made a large contribution to the subarctic ocean ecosystem (Jousé, 1962; Sancetta, 1982; Katsuki et al., 2003).

4.2 Temporal variations of the diatom groups

According to the results of stratigraphically-constrained cluster analysis (Grimm, 1987), the diatom record of core LV63-4-2 over the past 32 kyr can be divided into the following four assemblage zones (Figure 2):

4.2.1 Zone I (32–18 kyr BP)

This zone is dominated by the open-ocean cold-water diatoms *R. hebetata* (16.0–26.7%), *S. latimarginatus* (8.1–15.6%), *T. longissima* (12.0–20.0%), *C. marginatus* (9.6–16.0%) and the *Actinocyclus* group (4.8–15.5%). The coastal or ice-margin species, *T. gravida* resting spores, is also abundant (6.6–17.2%), but its abundance fluctuates. In contrast, the proportion of *N. seminae*, typical of the subarctic Pacific, is low in this zone (0.8–9.4%; Figure 3D). Although the proportion of the sea-ice species *F. cylindrus* is relatively low (< 5.5%), it reached its maximum level within the entire sequence (Figure 3H).

4.2.2 Zone II (18–15 kyr BP)

The diatom composition of this zone is relatively constant compared to Zone I (Figure 2). The proportion of most of the open-ocean cold-water species, such as *T. longissima, C. marginatus*, and *R. hebetata*, gradually decrease, while the ice-margin species *T. gravida* gradually increases, reaching ~20% at ~15 kyr BP (Figures 2, 3G). The abundance of the typical North Pacific indicator species *N. seminae* also increases continuously, reaching 26% at ~16 kyr BP (Figure 3D). However, freshwater and warm-water diatom species are absent in this zone (Figures 3E, F). In this zone, as in Zone I, the number of diatom species (species diversity) is very low. Generally, in the diatom communities of Zone I and Zone II, with unfavorable conditions and low nutrient concentrations, prolonged ice conditions and limiting factors resulted in few species, reduced species (taxonomic) richness, and the assemblage became monodominant: that is, 4–5 species had a high abundance and biomass.

4.2.3 Zone III (15–11.7 kyr BP)

The typical North Pacific species *N. seminae* is the most abundant species (47–54%) in this zone (Figure 3D). The sea-ice species *F. cylindrus* is absent, and the abundances of the cold-water species *S. latimarginatus* and the ice-margin species *T. gravida* sharply decrease and almost disappear. Additionally,

10.3389/fmars.2022.945110

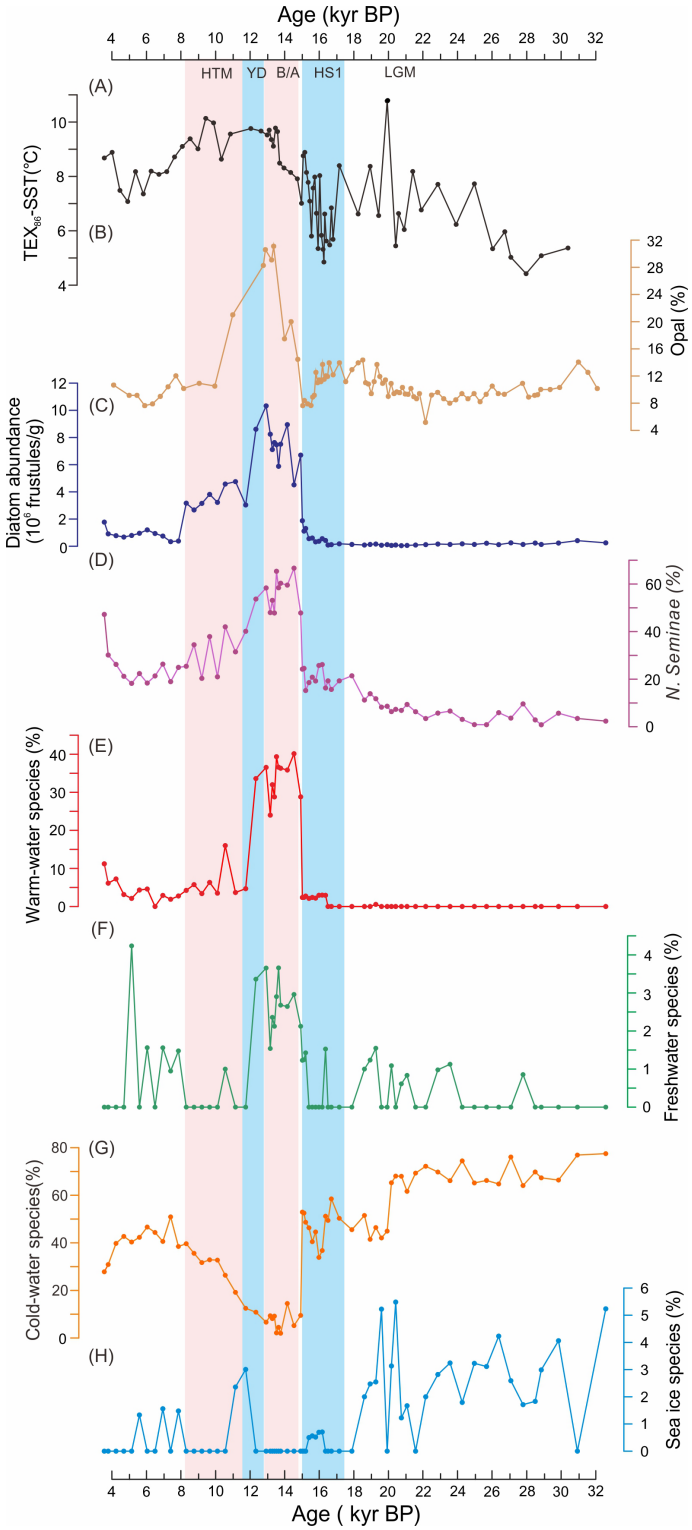

FIGURE 3
Records reflecting changes in sea surface temperature (SST) and biological production in core LV63-4-2 over the past 32 kyr: **(A)** TEX_{86}^{L} -SST, **(B)** opal concentration, **(C)** diatom abundances, **(D)** *Neodenticula seminae*, **(E)** warm-water species, **(F)** freshwater species, **(G)** cold-water species, and **(H)** sea-ice species. The pink and dark shading denote the warm intervals of the Bølling-Allerød [B/A] and the Holocene Thermal Maximum [HTM], respectively, and the blue shading denotes the cold intervals of Heinrich Stadial 1 [HS1] and the Younger Dryas stadial [YD].

there is the abrupt appearance and increase in the proportion of the warm-water species *T. nitzschioides*, *T. lineata*, *T. eccentrica*, *T. pacifica*, and *F. doliolus*, and of the freshwater species *G. oceanica* (2–4%), which reached a short-term maximum during 14.5–12 kyr BP.

4.2.4 Zone IV (11.7 kyr BP to present)

The abundance of the warm-water species decreased significantly after 11.7 kyr BP and remained relatively constant during the Holocene (Figure 3E). Freshwater diatoms were absent during 11–8 kyr BP but increased slightly thereafter (Figure 3F). The cold-water species *S. latimarginatus*, the ice-margin species *T. gravida*, and the typical North Pacific species *N. seminae*, were dominant during the Holocene, with an average abundance of 25% (Figure 3G). In contrast, sea-ice species were absent in this zone (Figure 3H). An increase in the content of the resting spores of diatoms of the genus *Chaetoceros* spp. was observed in the sediments of this zone.

4.3 Export productivity and sea surface temperature

Modern observations in the Subarctic Pacific have shown that total mass flux and biogenic opal flux are highly correlated (Honda et al., 2002), suggesting that opal and diatom assemblages are the main export productivity for organic carbon (Otosaka and Noriki, 2005). The diatom abundance was very low (0.04–1.31×10^6 frustules/g) between 32 and 15 kyr BP (Figure 3C). However, it then increased abruptly, from 1.11 to 10.33×10^6 frustules/g, at ~14.5 kyr BP, and remained relatively high until 11.7 kyr BP. Subsequently, the diatom abundance decreased gradually from 4.75 to 0.38×10^6 frustules/g during 11–8 kyr BP and remained at a low level thereafter. The biogenic opal concentration was low during 32–15 kyr BP, with an average of 10.5%, but it increased abruptly after 15 kyr BP (Yao et al., 2022; Figure 3B). Higher values were maintained during 14.7–10.5 kyr BP, with an average of 24.1%, reaching a peak of 31.2% at ~13 kyr BP. The opal concentration then decreased and remained relatively uniform at 9% during 10–2 kyr BP (Figure 3B). There is a strong correlation between changes in the biogenic opal and diatom abundance ($r=0.82$, $p<0.01$; Figures 3C, B), which suggests that diatoms were the main components of the biogenic material in the subarctic NW Pacific in the last 32 kyr.

The TEX_{86}^{L} records reveals that SST ranged from 4 to 10.8°C in the core LV63-4-2 during the last 32 kyr (Figure 3A). The TEX_{86}^{L} -based SST ($SST_{TEX_{86}^{L}}$) increased gradually from 5.0 to 10.8°C during 30–19 kyr BP, but with a brief decrease from 8.2 to 5.4°C during 22–20 kyr BP. The SST then decreased substantially, from 8.4 to 5.3°C, during 19–16 kyr BP, followed by a rapid increase after 16 kyr BP. Higher SSTs, from 8.2 to 10.1°C, continued during 14–8 kyr BP, followed by a modest decrease during 8–4 kyr BP (Figure 3A).

5 Discussion

The records of diatom assemblages and $SST_{TEX_{86}^{L}}$ for the interval of 32-26 kyr BP (which records a minimum in $SST_{TEX_{86}^{L}}$) (Figures 2, 3) are inconsistent with comparable records from the North Pacific, and therefore the subsequent discussion focuses on the interval from 26 kyr BP to the present.

5.1 Possible mechanisms driving productivity variations in the Subarctic Pacific Ocean

5.1.1 Last Glacial Maximum (23–18 kyr BP)

In general, extensive sea-ice, low productivity, and moderately warm SSTs occurred in the subarctic NW Pacific during the LGM (Figure 4), in contrast with the lowest SST which occurred during 32-26 kyr BP (Figures 2, 3). There was no significant decrease in $SST_{TEX_{86}^{L}}$ during the LGM (Figure 4A), which is supported by a warm SSTs reconstructed from diatom and $\delta^{18}O$ records from core MD01-2416 (Figure 5D; Gebhardt et al., 2008). However, the maximum proportion of sea-ice diatoms in core LV63-4-2 (Figure 4E) points to extensive sea-ice coverage in the subarctic NW Pacific during this period, as evidenced by the lowest proportion of warm-water diatom species and the fluctuating increase in the ice-margin species *T. gravida*. The presence of ice-related diatoms in core ES (49.73° N, 168.32°E; 2,388 m water depth) from the NW Pacific further indicates the occurrence of sea-ice in this area (Katsuki and Takahashi, 2005). In addition, ice proxy 25 (IP_{25}) concentrations in cores SO202-07-6 (51.3°N, 167.7°E; 2,345 m water depth; Figure 4D) and SO202-27-6 (54.2°N, 149.6°W; 2,919 m water depth) from the NW and northeastern (NE) Pacific Ocean both increased during the LGM, which demonstrates the distribution of sea-ice throughout the subarctic region (Méheust et al., 2018). Nevertheless, diatom records from the Bering Sea and subarctic Pacific show that core ES from the western subarctic Pacific contained a higher proportion of open-water diatoms and fewer ice-related diatoms compared to the cores from the eastern Bering Sea during the LGM. This indicates that seasonal sea-ice prevailed in the western Bering Sea and subarctic Pacific during the LGM, whereas in the eastern Bering Sea more stable and persistent sea-ice conditions occurred (Katsuki et al., 2003).

Low biological productivity during the LGM is indicated by the lowest biogenic opal content and diatom abundance in core LV63-4-2 (Figures 3B, C). According to Artemova et al. (2018), very cold climatic conditions and low bio-productivity in the Sea of Okhotsk occurred during Marine Isotope Stage 2 until 21 kyr BP. Low concentrations of sterols in core SO202-27-6 also point

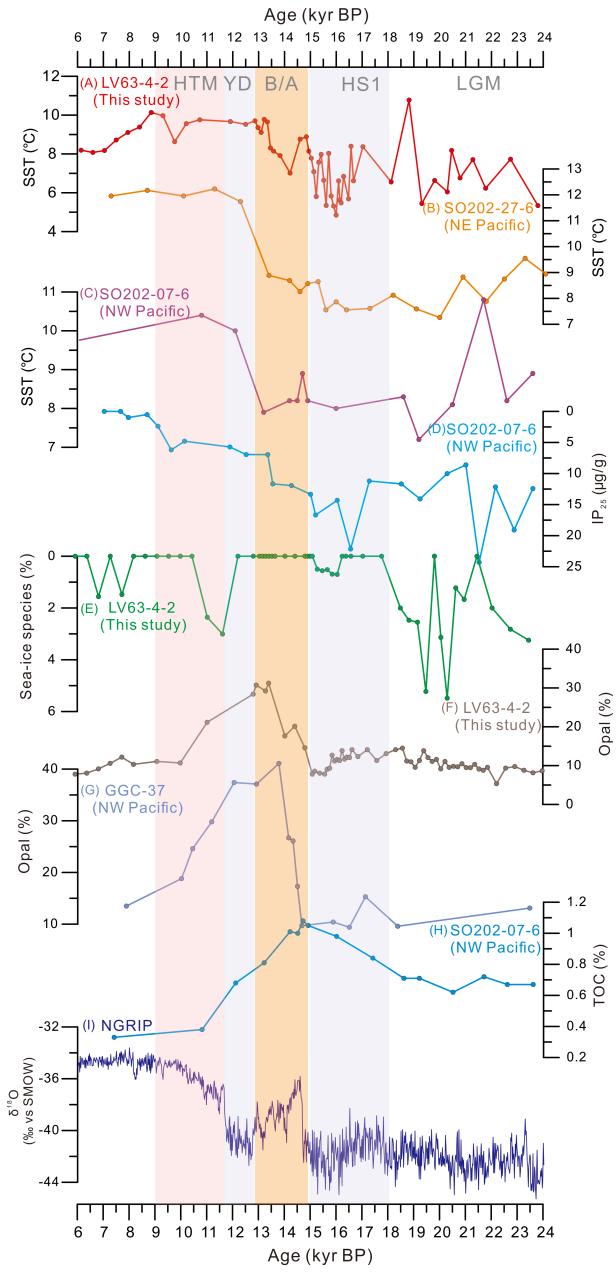

FIGURE 4
Comparison of paleoenvironmental proxies between core LV63-4-2 and other regional records. **(A–C)**: Sea surface temperature (SST) records from cores LV63-4-2, SO202-27-6 (Maier et al., 2015), and SO202-07-6 (Serno et al., 2015). Sea-ice proxies: **(D)** Ice proxy 25 (IP_{25}; μg/g) concentration from core SO202-07-6. **(E)** Abundance of sea-ice diatom species from core LV63-4-2. Paleoproductivity proxies: **(F)** Opal concentration (%) from core LV63-4-2; **(G)** Opal content (%) of core GGC-37 (Keigwin et al., 1992); **(H)** Total organic carbon (TOC; wt.%) from core SO202-07-6 (Serno et al., 2015); and **(I)** $\delta^{18}O$ record of the North Greenland Ice Core Project (NGRIP) ice core (‰; Rasmussen et al., 2006).

to reduced productivity in the eastern subarctic Pacific at this time (Méheust et al., 2018). Additionally, a decrease in the biogenic opal concentration during the LGM was also observed in core RAMA-44PC (53°N, 164.65°E; 2,980 m water depth) from the NW Pacific (Keigwin et al., 1992). The upwelling of Pacific Deep Water was weaker in the study area during glacial periods, and it also shifted southward (Narita et al., 2002). Therefore, the decreased biological productivity in the subarctic NW Pacific region was likely caused by the combination of a reduced nutrient supply due to weakened/

retreated North Pacific upwelling and an extended sea-ice cover during the LGM (Narita et al., 2002). Therefore, the supply of nutrients was low during glacial periods and biological productivity was reduced (Narita et al., 2002), which is consistent with the low biogenic opal concentration and diatom abundance in core LV63-4-2 (Figure 4F).

5.1.2 Heinrich Stadial 1 (~17.5–14.9 kyr BP)

The $SST_{TEX_{86}^{L}}$ record indicates that the SST during 18.0–15.0 kyr BP, corresponding to Heinrich Stadial 1 (HS1) (Hemming, 2004; Naafs et al., 2013), was generally colder than during the LGM (Figure 4A). In addition, the oxygen isotope record from the Greenland ice cores indicates that colder climatic conditions occurred during HS1 than during the LGM (Rasmussen et al., 2006; Figure 4I). However, the abrupt decrease in the sea-ice-related diatom abundance during this interval indicates the onset of deglaciation and the occurrence of open water in the subarctic NW Pacific, which was barely affected by sea-ice (Figure 4E). This inference is supported by the high proportion of the open-ocean cold-water species *S. latimarginatus* in core LV63-4-2 (Figures 2 and 3G), and by the low abundance of sea-ice related diatoms in the Bering Sea and the subarctic NW Pacific during HS1 (Caissie et al., 2010; Max et al., 2012). These records suggest that extensive sea-ice production in the Arctic Ocean resulted in the decreased export of sea-ice from the Arctic Ocean, and subsequently to a pronounced reduction of drifting ice in the subarctic Pacific from the LGM to the HS1.

The low biogenic opal content and diatom abundance indicate constant low productivity throughout HS1, showing the same pattern as that during the LGM (Figures 3B, C). A low biogenic opal content was also observed in the western subarctic Pacific (core SO201-2-12KL) and in the Bering Sea (core SO201-2-77KL), suggesting reduced biological productivity, most likely caused by marginal sea-ice cover (Méheust et al., 2015). In addition, the slight increase in the high-nutrient indicator species *N. seminae* and in the $SST_{TEX_{86}^{L}}$ record indicate a temperature increase from 5.8°C to 8°C after ~16.0 kyr BP (Figures 3D and 4A), which is in good agreement with the occurrence of open water in the subarctic NW Pacific. These observations suggest that primary productivity began to increase at the end of HS1, which is consistent with the increase in the total organic carbon (TOC) content of core SO202-07-6 during the same period (Figure 4H; Méheust et al., 2015), indicating the early stage of the last deglaciation.

5.1.3 Bølling/Allerød warm interstadial (14.7–12.8 kyr BP)

There was a rapid increase in the $SST_{TEX_{86}^{L}}$ during 14.7–12.8 kyr BP, corresponding to the B/A (Figure 4A). Abrupt changes in the diatom composition at the HS1-B/A boundary (~14.7 kyr BP) occurred across the entire northern Pacific, as well as in the Bering Sea (Katsuki and Takahashi, 2005; Takeda and Tsuda, 2005; Max et al., 2012). Also, rapid increases in freshwater and warm-water diatoms (to ~40%; Figures 3E, F), and in the typical Pacific indicator species *N. seminae* species (from 10% to 65%; Figure 3D), during this period indicate a pronounced amelioration of regional climatic conditions and the enhancement of the AS, which was coeval with a rise in sea level (Gorbarenko and Malakhova, 2021). The increase in the warm-water species suggests a probable northward shift of the subtropical water masses and an increase in the penetration of warm-water masses towards the Detroit Seamount from the low-latitude Pacific, with the Kuroshio Current (Lembke-jene et al., 2018). The study area at this time was likely affected by both subarctic and subtropical water masses, possibly creating a frontal zone of subtropical and subarctic gyres, where a zone of water mixing occurred and high productivity was created (Venrick, 1971). Changes in the diatom assemblages from the nearby core MD01-2416 also show an increase in freshwater and warm-water species during this period (Gebhardt et al., 2008). Additionally, the large-scale melting of sea-ice from the decay of the Kamchatka glaciers may have led to the influx of large amounts of river and glacial meltwater to the subarctic NW Pacific (Gorbarenko et al., 2019).

High proportions of *N. seminae*, which is a reliable tracer of the nutrient-rich AS (Sancetta, 1982), suggest high biological productivity in the SPO during the B/A interstadial (Figure 3D). This is supported by a major increase in the biogenic opal content and the highest diatom abundance in core LV63-4-2 occured at this time (Figures 3B, C). In addition, deglacial meltwater incursions in the Aleutian Current and silica input from North American rivers promoted increased productivity in the North Pacific after ~15.5 kyr BP (Gebhardt et al., 2008). Numerous observations also confirm a rapid rise in the SST and collapse of NPIW, which promoted a large increase in biological productivity (Lam et al., 2013; Gray et al., 2018). The maximum TOC values and increases in the phytoplankton biomarker concentrations of cores SO202-07-6 (Figure 4H, Méheust et al., 2015) and SO202-27-6 reflect the enhancement of biological productivity in the subarctic Pacific. This high-productivity event was also reported in the NW Pacific (Keigwin et al., 1992; Gebhardt et al., 2008) and in the NE Pacific (Gebhardt et al., 2008) during 15.8–13.3 kyr BP.

5.1.4 The Holocene and Younger Dryas (12.8 kyr BP to the present)

Despite a stable and nonsignificant decrease in SST records in the subarctic NW Pacific during the Younger Dryas (YD) stadial (12.8–11.7 kyr BP; Figure 3A), a YD-like cold event is indicated by a sudden rise in the sea-ice diatom species and a dramatic decrease in warm-water and freshwater species (Figures 3H, E, F). Additionally, the SST reconstruction for the nearby core MD01-2416 shows a small cooling event in the study area during the YD stadial (Gebhardt et al., 2008). The reason for this discrepancy in

temperature is likely to be the seasonality of different proxies, as diatom reconstructions are mainly used for summer and GDGTs-based SST estimates are used for annual temperature (Müller et al., 1998). In the western Pacific, a slight increase in the IP_{25} concentration probably reflects occasional sea-ice incursions in the area (Méheust, 2014). However, in the eastern subarctic Pacific (core SO202-27-6), the lack of IP_{25} and minimal IP_{25} values at the onset of the YD show an inverse pattern (Méheust et al., 2018). A rapid decrease in the biogenic opal content and the proportion of *N. seminae*, together with reduced diatom abundance and diversity, also support a YD-like cold event in the subarctic NW Pacific (Figure 3). A decrease in productivity is also suggested by the decrease in the biogenic opal in cores SO201-2-12KL and SO201-2-77KL, and by the reduced TOC content in core SO202-07-6 (Figure 4H; Riethdorf et al., 2013; Méheust, 2014). Hence, as in the western subarctic Pacific, previous studies based on biogenic opal and TOC content also point to occasional sea-ice occurrences which limited the primary productivity during the YD.

During the early Holocene (11–9 kyr BP) there was a decrease in $SST_{TEX^L_{86}}$ in core LV63-4-2, which reached 10°C in the subarctic NW Pacific (Figure 4A), corresponding to the Holocene Thermal Maximum (HTM), which is supported by the disappearance of sea-ice diatom species in the core (Figure 4E). In the western Bering Sea, an abrupt decrease in IP_{25} (cores SO201-2-114KL and SO201-2-77KL) also indicates reduced sea-ice or ice-free conditions during the Holocene. Reduced sea-ice was also recorded by the diatom composition of core SO201-2-12KL (Méheust, 2014). Concurrently, the highly variable abundance of *N. seminae* suggestes several incursions of AS water into the subarctic NW Pacific during the HTM (Figures 3D). Notably, there is an increase in the proportion of the shallow marine transported mesohalobic species *Odontella aurita* in the diatom assemblage, which is associated with transport from shallower areas of the shelf, indicating periods of active lateral inflow, which may have been associated with the increased influence of currents or drifting sea-ice.

From 8.3 kyr BP onwards, a substantial decrease in $SST_{TEX^L_{86}}$ (by ~3°C; Figure 4A), and a ~3°C fall in alkenone SST was recorded in core SO202-07-6 (Méheust et al., 2018), indicating a cooling trend in the Holocene in the subarctic NW Pacific (Figure 4C). A prominent cooling event was also observed at high latitudes during this interval (Alley et al., 1997; Clarke et al., 2004). Thereafter, decreased SSTs were also reconstructed from cores RAMA44 and MD02-2486 from the western and eastern North Pacific, respectively (Keigwin et al., 1992). Additionally, a substantial increase in the IP_{25} concentration in core SO202-18-6 from the continental shelf of the northeastern Bering Sea was recorded after 8.5 kyr BP, and it remained at a high level during the mid-Holocene (Méheust et al., 2018). Various Holocene climatic records from the North Pacific were reviewed by Max et al. (2012), and they demonstrate a consistent cooling trend since 7 kyr BP, which is consistent with the $SST_{TEX^L_{86}}$ record of core LV63-4-2. Moreover, sea-ice diatom species almost disappeared during the Holocene (Figure 4E) and IP_{25} was almost absent in cores SO202-07-6 (Figure 4D) and SO202-27-6 (Maier et al., 2015), suggesting ice-free conditions in the subarctic Pacific.

Low biological productivity during the Holocene is reflected by low diatom abundances, both in the western North Pacific (cores LV63-4-2, MD01-2416, and RAMA44) and in the eastern North Pacific (core MD01-2489; Gebhardt et al., 2008), and by low biogenic opal concentrations in cores LV63-4-2 and SO202-07-6 from the NW Pacific (Méheust, 2014; Figure 5C). In addition, a prominent halocline developed in the subarctic North Pacific at ~11.1 kyr BP (or at 9.3 kyr BP), which limited the transport of deep water to the surface and weakened the deep-ocean transport of nutrients (Haug et al., 1999), possibly resulting in low productivity in the subarctic North Pacific from the onset of the Holocene. Notably, the proportion of freshwater diatoms increased gradually during 8–6 kyr BP (Figure 5E). The surrounding continental area did not supply major fluvial runoff and neither did it contain large ice sheets to sustain continuous meltwater discharge (Sarnthein et al., 2006). Therefore, we infer that the increased representation of freshwater diatoms was likely the result of the influence of fluvial runoff from the Kamchatka Peninsula and the low-salinity Aleutian Current in the study area (Sarnthein et al., 2004; Riethdorf et al., 2013).

5.2 Deglacial upwelling, productivity, and CO_2 outgassing in the North Pacific Ocean

Although the glacial/interglacial changes in paleoceanographic conditions in the Southern Ocean and Subarctic Pacific (Jaccard et al., 2010) were similar, these two regions exert different controls on heat transport, marine biological productivity, and ocean-atmospheric CO_2 exchange (Sigman et al., 2021). The degassing of CO_2 from the Southern Ocean during the last deglaciation was related to the upwelling of CO_2-enriched deep waters, which was interrupted by the Antarctic Cold Reversal (Skinner et al., 2010; Burke and Robinson, 2012). These processes are generally assumed to have played a dominant role in the deglacial rise in atmospheric pCO_2 of ~90 ppm (Schmitt et al., 2012; Parrenin et al., 2013; Marcott et al., 2014). These warm intervals coincided with HS1 and the YD, when the Northern Hemisphere experienced abrupt cooling and a weakening or collapse of the Atlantic meridional overturning circulation (Figure 5J; McManus et al., 2004; Bohm et al., 2015). The corresponding slowdown of northward heat transport led to the warming of the Southern Hemisphere and consequently to the southward shift of the westerly wind belt (Toggweiler and Lea, 2010). Anderson et al. (2009) suggested that the shifts in the Antarctic Polar Front

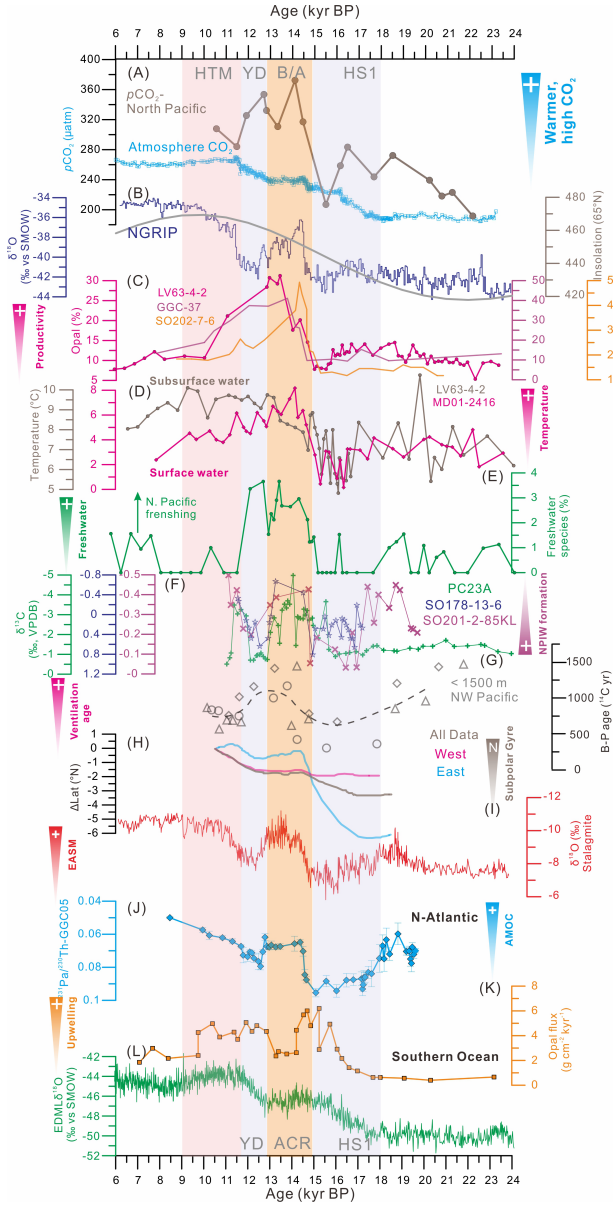

FIGURE 5
Comparison between northern and southern hemispheric processes for the last glacial termination. **(A)** Atmosphere pCO_2 (Marcott et al., 2014) and the near-surface subpolar North Pacific (Gray et al., 2018). **(B)** $\delta^{18}O$ record of the North Greenland Ice Core Project (NGRIP) ice core (NGRIP Dating Group, 2006) and insolation at 65°N, as references Northern Hemisphere climate signals. **(C)** Opal content (%) of cores LV63-4-2 (this study), GGC-37 (Keigwin et al., 1992), and SO202-7-6 (Serno et al., 2015). **(D)** Sea surface temperature (SST) records from cores LV63-4-2 and MD01-2416 (Gebhardt et al., 2008). **(E)** Freshwater diatom species in core LV63-4-2. **(F)** $\delta^{13}C$ record of *Cibicidoides* spp. (versus the Vienna Pee Dee Belemnite) from the intermediate Bering Sea (SO201-2-85KL) and Okhotsk Sea (SO178-13-6; Max et al., 2014). **(G)** Benthic-planktonic (B-P) ^{14}C age difference at the intermediate depths (< 1,500 m) in the northwest Pacific (NW Pacific): core CH84-14 (circles), core GH02-1030 (triangles), and core MR01K03-PC4/PC5 (diamonds; Okazaki et al., 2010). **(H)** Reconstructed changes in the position of the subpolar gyre boundary (Gray et al., 2020). **(I)** Chinese speleothem $\delta^{18}O$ record (Cheng et al., 2016). **(J)** $^{231}Pa/^{230}Th$ ratio on the Bermuda Rise (McManus et al., 2004). **(K)** Opal flux records from South Atlantic sediment core TN057-13PC4, showing changes in the upwelling of nutrient-rich deep water (Anderson et al., 2009). **(L)** $\delta^{18}O$ record of the European Project for Ice Coring in Antarctica (EPICA) Dome C (EPICA Community Members, 2006), as a reference Southern Hemisphere climate signal. Abbreviations: HS1, Heinrich Stadial 1; YD, Younger Dryas Stadial; BA, Bølling-Allerød; N. Pacific, North Pacific; N-Atlantic, North Atlantic; and ACR, Antarctic Cold Reversal.

caused a strengthening of wind-driven upwelling and led to higher productivity during HS1 and the YD (Figure 5K). These mechanisms are supported by the close relationship between atmospheric pCO_2 (Figure 5A) and Antarctic temperatures (Figure 5L). However, Southern Hemisphere processes cannot explain some of the CO_2 equilibrium states during the B/A intervals, and several studies have suggested that the CO_2 may also have degassed from the deglacial subarctic Pacific (Lam et al., 2013; Rae et al., 2014), which is characterized by CO_2-rich deep water (Figure 5A).

A distinct and large increase in productivity during the B/A interstadial (14.7–12.9 kyr BP) was recorded in sediment cores from the SPO (LV63-4-2, GGC-37, and SO202-7-6) (Figure 5C), indicated by high accumulation rates of biogenic opal (Lam et al., 2013). These high biogenic accumulation rates could have contributed to the reduced oxygen concentrations at intermediate depths in the NW Pacific, which were related to the substantial weakening of the NPIW and the expansion of the oxygen minimum zone at the intermediate-water level (Crusius et al., 2004; Schmittner et al., 2007; Chikamoto et al., 2012). Deglacial high biological productivity is also indicated by the occurrence of laminated and biogenic opal-rich sediments and an increase in open-water diatoms in sediments from the western Bering Sea (Max et al., 2012; Riethdorf et al., 2013). Large-scale deep water upwelling results in the mixing of nutrient-rich intermediate and deep water (Gray et al., 2018), which can trigger a productivity explosion. The greatly reduced NPIW formation at the onset of the B/A also weakened the upper-water stratification of the SPO, which accelerated the upwelling of nutrient-rich Pacific deep water, thus increasing the biological productivity (Sarnthein et al., 2006; Rella et al., 2012; Ren, 2015). Further support for a deglacial increase in export production comes from $\delta^{13}C$ measurements of epibenthic foraminifera throughout the subarctic Pacific and the Bering Sea (Rella et al., 2012; Max et al., 2014), indicating a basin-wide increase of the rate at which nutrients were supplied to the surface ocean (Figure 5F).

The timing and magnitude of the changes in productivity are supported by other independent reconstructions from the mid-to-high latitudes in the North Pacific Ocean (Okazaki et al., 2010). This is supported by a compilation of radiocarbon ages for the NW Pacific (Figure 5G; at water depths< 1500 m), which reflect the deep ventilation of NPIW transport (Okazaki et al., 2010). Specifically, high benthic-planktic events were initiated during strong monsoon intervals, whereas low benthic-planktic events tended to occur in concert with weak monsoons (Figures 5G, I). This is further supported by recent radiocarbon and sedimentological results from the Gulf of Alaska, which indicate the role of moisture and heat transport from low latitudes in the paleoclimate of the North Pacific (Walczak et al., 2020). However, warming in the North Pacific, *via* a northward diversion of the polar front, could also have driven changes in oceanic heat transport, supporting increasing benthic-planktic offsets after the B/A interstadial (Gray et al., 2020). Temperature fluctuations in the thermocline depth indicated by our TEX_{86}^{L} record (Figure 5D) are typically attributed to spatial shifts in the Subpolar Front, as an expansion of the front would increase thermocline warming and northward heat transport to the Subarctic Gyre. The observed warming of the subpolar North Pacific by 5°C from ~16.5 kyr BP, during the interval of increasing Northern Hemisphere insolation (Figure 5B), would have promoted a decrease in the pole-to-equator temperature gradient and a northward shift of the westerly jet (Figure 5H; Gray et al., 2020). This in turn led to enhanced moisture transport and an increase in the annual mean precipitation over the ice sheets, contributing to the net negative mass balance and the retreat of the marine margin of the Kamchatka glaciers and the Cordilleran Ice Sheet (Walczak et al., 2020; Gorbarenko et al., 2022). This scenario is consistent with evidence for the presence of freshwater diatom species observed in core LV63-4-2 (Figure 5E), representing meltwater fluxes from the Kamchatka glaciers and Cordilleran Ice sheet. In general, increased subsurface heat advection to the Subarctic Gyre would lead to weaker thermocline stratification in the western and northeastern Pacific, thus creating a subsurface channel for latitudinal heat transport *via* the deep thermocline.

Additional evidence attributes the interaction between Pacific and Atlantic ice sheet retreat events to atmospheric heat transport and adjustments in the Arctic (Praetorius et al., 2018), especially the net freshwater transport from the Pacific to the Arctic when the Bering Strait is open, and/or rapid sea-level rises from ice melting (Praetorius et al., 2020). Increased heat transport from a more tilted subarctic gyre could explain the anomalous warmth of the SPO during the B/A interstadial and it may have driven wider Northern Hemisphere warming and the mountain glaciers and ice sheet collapses at this time (Lora et al., 2016). The increase in the pCO_2 within the near-surface ocean at the onset of the B/A interstadial would have resulted in significant outgassing of CO_2, with the previously reconstructed ocean-atmosphere pCO_2 difference being ~130 µatm (Gray et al., 2018; Figure 5A). Also, the release of CO_2 from the subpolar Pacific at the onset of the B/A may have contributed to the rapid (~10 µatm) increase in atmospheric CO_2 which was observed at this time. Although some portion of this CO_2 drawdown may have been countered by carbonate compensation, it is likely that other mechanisms, such as changes in iron fertilization and destratification in the Southern Ocean (Figure 5K), may also have operated to offset this CO_2 fall and to achieve the observed deglacial CO_2 rise. Overall, our study demonstrates that changes in the mid-depth circulation of the NW Pacific may have played a crucial role in

glacial nutrient availability and biological productivity in the NW Pacific, and intensified the release of CO_2 from the subpolar Pacific during the warm intervals may have contributed to the breakdown of stratification in the North Pacific.

6 Conclusions

The modern SPO is strongly stratified by a buoyant, low-salinity surface layer, which is sustained by an excess in precipitation and runoff relative to evaporation, and restricted meridional exchange between subpolar and subtropical surface waters. We present a centennial-to-millennial-scale record of changes in the vertical mixing of water masses, SST, and paleoproductivity from core LV63-4-2, in the subarctic NW Pacific, during the LGM. The results showed that productivity, inferred by the low biogenic opal concentration and diatom abundance, was low in the subarctic NW Pacific region, possibly because of the extended sea-ice cover and weakened vertical mixing of water masses during the LGM. Moreover, the deglaciation accelerated at the onset of the B/A interval, leaving the subarctic Pacific and Bering Sea-ice-free, and coinciding with high $SST_{TEX^{L}_{86}}$ and maximum productivity, possibly due to the vertical admixture of old, nutrient-rich Pacific deep water and nutrient-depleted surface water. We propose that the strengthening of the subpolar gyre would have increased the poleward heat transport, warming the high latitudes and suppressing the formation of the NPIW. Overall, our results indicate that past changes in the NW Pacific mid-depth circulation may have played a crucial role in glacial nutrient availability and biological productivity in the NW Pacific. This inference supports the notion that CO_2 outgassing from the North Pacific helped to maintain high atmospheric CO_2 concentrations during the B/A interstadial and contributed to the deglacial CO_2 rise.

Data availability statement

The original contributions presented in the study are included in the article/Supplementary Material. Further inquiries can be directed to the corresponding authors.

Author contributions

YL, YQ, LS, and YiZ designed the study, synthesized and analyzed the data, and wrote the manuscript with contributions from all authors. SG, QL helped to build the age model. AA and YuZ helped in diatom and GDGTs analyses, respectively. AB, DZ helped in data interpretation. All authors contributed to the manuscript and approved its submission. All authors contributed to the article and approved the submitted version.

Funding

This work was supported jointly by the Marine S&T Fund of Shandong Province for Pilot National Laboratory for Marine Science and Technology (Qingdao) (No. 2022QNLM050203), Program of State Key Laboratory of Marine Geology, Tongji University (No. MGK202209), National Natural Science Foundation of China (NSFC) (No. U1606401, 41876215, 42176226) and in part by the Taishan Scholar Program of Shandong (XF Shi).

Acknowledgments

We thank the crew, captain and scientists of R/V "*Akademik M.A. Lavrentyev*" for their efforts in collecting the sediment samples from the Northwest Pacific during the joint Russian-Chinese cruise in 2013. We thank Jan Bloemendal for improving the English language.

Conflict of interest

The authors declare that the research was conducted in the absence of any commercial or financial relationships that could be construed as a potential conflict of interest.

Publisher's note

Supplementary material

The Supplementary Material for this article can be found online at: https://www.frontiersin.org/articles/10.3389/fmars.2022.945110/full#supplementary-material

References

Alley, R. B., Mayewski, P. A., Sowers, T., Stuiver, M., Taylor, K. C., and Clark, P. U. (1997). Holocene Climatic instability: A prominent, widespread event 8200 yr ago. *Geology* 25, 483–486. doi: 10.1130/00917613(1997)025<0483:HCIAPW>2.3.CO;2

Anderson, R. F., Ali, S., Bradtmiller, L. I., Nielsen, S. H. H., Fleisher, M. Q., Anderson, B. E., et al. (2009). Wind-driven upwelling in the southern ocean and the deglacial rise in atmospheric CO_2. *Science* 323, 1443–1448. doi: 10.1126/science.1167441

Antonov, J. I., Seidov, D., Boyer, T. P., Locarnini, R. A., Mishonov, A. V., Garcia, H. E., et al. (2010). World ocean atlas 2009, vol. 2, salinity. *NOAA Atlas NESDIS* 69, 184. doi: 10.13140/2.1.1115.4889

Artemova, A. V., Sattarova, V. V., and Vasilenko, Y. P. (2018). Distribution of diatoms and geochemical features of holocene sediments from the kuril basin (Sea of Okhotsk). *Deep Sea Res. Part II: Topical Stud. Oceanography* 154, 10–23. doi: 10.1016/j.dsr2.2017.12.019

Basak, C., Fröllje, H., Lamy, F., Gersonde, R., Benz, V., Anderson, R. F., et al. (2018). Breakup of last glacial deep stratification in the south pacific. *Science* 359, 900–904. doi: 10.1126/science.aay8178

Bohm, E., Lippold, J., Gutjahr, M., Frank, M., Blaser, P., Antz, B., et al. (2015). Strong and deep Atlantic meridional overturning circulation during the last glacial cycle. *Nature* 517, 73–76. doi: 10.1038/nature14059

Broecker, W. S. (1990). Salinity history of the northern Atlantic during the last deglaciation. *Paleoceanography* 5, 459–467. doi: 10.1029/PA005i004p00459

Burke, A., and Robinson, L. F. (2012). The southern ocean's role in carbon exchange during the last deglaciation. *Science* 335, 557–561. doi: 10.1126/science.1208163

Caissie, B., Brigham-Grette, J., Lawrence, K., Herbert, T., and Cook, M. (2010). Last glacial maximum to Holocene sea surface conditions at umnak plateau, Bering Sea, as inferred from diatom, alkenone, and stable isotope records. *Paleoceanography* 25, 1206. doi: 10.1029/2008PA001671

Cheng, H., Edwards, R. L., Sinha, A., Spotl, C., Yi, L., Chen, S., et al. (2016). The Asian monsoon over the past 640,000 years and ice age terminations. *Nature* 534, 640–646. doi: 10.1038/nature18591

Chen, W., Mohtadi, M., Schefuß, E., and Mollenhauer, G. (2014). Organic-geochemical proxies of sea surface temperature in surface sediments of the tropical eastern Indian ocean. *Deep Sea Res. Part I: Oceanographic Res. Papers.* 88, 17–29. doi: 10.1016/j.dsr.2014.03.005

Chikamoto, M. O., Menviel, L., Abe-Ouchi, A., Ohgaito, R., Timmermann, A., Okazaki, Y., et al. (2012). Variability in north pacific intermediate and deep water ventilation during Heinrich events in two coupled climate models. *Deep Sea Res. Part II: Topical Stud. Oceanography* 61, 114–126. doi: 10.1016/j.dsr2.2011.12.002

Church, M. J., Wai, B., Karl, D. M., and DeLong, E. F. (2010). Abundances of crenarchaeal amoA genes and transcripts in the pacific ocean. *Environ. Microbiol.* 12, 679–688. doi: 10.1111/j.1462-2920.2009.02108.x

Clarke, G. K. C., Leverington, D. W., Teller, J. T., and Dyke, A. S. (2004). Paleohydraulics of the last outburst flood from glacial lake agassiz and the 8200BP cold event. *Quaternary Sci. Rev.* 23, 389–407. doi: 10.1016/j.quascirev.2003.06.004

Crosta, X., Romero, O., Armand, L. K., and Pichon, J.-J. (2005). The biogeography of major diatom taxa in southern ocean sediments: 2. open ocean related species. *Palaeogeography Palaeoclimatol. Palaeoecol.* 223, 66–92. doi: 10.1016/j.palaeo.2005.03.028

Crusius, J., Pedersen, T. F., Kienast, S., Keigwin, L., and Labeyrie, L. (2004). Influence of northwest pacific productivity on north pacific intermediate water oxygen concentrations during the bølling-allerød interval (14.7–12.9 ka). *Geology* 32, 633–636. doi: 10.1130/G20508.1

Davis, C. V., Myhre, S. F., Deutsch, C., Caissie, B., Praetorius, S., Borreggine, M., et al. (2020). Sea Surface temperature across the subarctic north pacific and marginal seas through the past 20,000 years: A paleoceanographic synthesis. *Quaternary Sci. Rev.* 246, 106519. doi: 10.1016/j.quascirev.2020.106519

Dodimead, A. J., Favorite, F., and Hirano, T. (1963). Review of oceanography of the subarctic pacific region. *Int. North Pac. Fish. Commun. Bull.* 13, 1–195.

Dong, L., Li, Q., Li, L., and Zhang, C. L. (2015). Glacial–interglacial contrast in MBT/CBT proxies in the south China Sea: Implications for marine production of branched GDGTs and continental teleconnection. *Organic Geochem.* 79, 74–82. doi: 10.1016/j.orggeochem.2014.12.008

Emile-Geay, J., Cane, M. A., Naik, N., Seager ,R., Clement,A.C., and van Geen, A. (2003). Warren revisited: Atmospheric freshwater fluxes and "Why is no deep water formed in the north pacific". *J. Geophys. Res.* 108, 3178. doi: 10.1029/2001jc001058

EPICA Community Members (2006). One-to-one coupling of glacial climate variability in Greenland and Antarctica. *Nature* 444, 195–198. doi: 10.1038/nature05301

Galbraith, E. D., Jaccard, S. L., Pedersen, T. F., Sigman, D. M., Haug, G. H., Cook, M., et al. (2007). Carbon dioxide release from the north pacific abyss during the last deglaciation. *Nature* 449, 890–893. doi: 10.1038/nature06227

Gebhardt, H., Sarnthein, M., Grootes, P. M., Kiefer, T., Kuehn, H., Schmieder, F., et al. (2008). Paleonutrient and productivity records from the subarctic north pacific for pleistocene glacial terminations I to V. *Paleoceanography* 23, PA4212. doi: 10.1029/2007pa001513

Gogorev, R. M. (2013). Centric diatoms (Bacillariophyta) from the Antarctic ocean. *Novosti Sist. Nizsh. Rast.* 47, 37–53. doi: 10.31111/nsnr/2013.47.37

Gorbarenko, S., and Malakhova, G. (2021). Orbital and suborbital environmental changes in the Western Bering Sea during the last 172 ka inferred from diatom and productivity proxies. *Global Planetary Change* 198, 103405. doi: 10.1016/j.gloplacha.2020.103405

Gorbarenko, S. A., Shi, X., Liu, Y., Vasilenko, Y. P., Yanchenko, E. A., Derkachev, A. N., et al. (2022). Iceberg discharge events in the northwest pacific and related sequence of kamchatka glaciations over the last 190 kyr. *Quaternary Sci. Rev.* 278, 107349. doi: 10.1016/j.quascirev.2021.107349

Gorbarenko, S., Shi, X., Zou, J., Velivetskaya, T., Artemova, A., Liu, Y., et al. (2019). Evidence of meltwater pulses into the north pacific over the last 20 ka due to the decay of kamchatka glaciers and cordilleran ice sheet. *Global Planetary Change* 172, 33–44. doi: 10.1016/j.gloplacha.2018.09.014

Gray, W. R., Rae, J. W. B., Wills, R. C. J., Shevenell, A. E., Taylor, B., Burke, A., et al. (2018). Deglacial upwelling, productivity and CO_2 outgassing in the north pacific ocean. *Nat. Geosci.* 11, 340–344. doi: 10.1038/s41561-018-0108-6

Gray, W. R., Wills, R. C. J., Rae, J. W. B., Burke, A., Ivanovic, R. F., Roberts, W. H. G., et al. (2020). Wind-driven evolution of the north pacific subpolar gyre over the last deglaciation. *Geophys. Res. Lett.* 47, e2019GL086328. doi: 10.1029/2019gl086328

Grimm, E. C. (1987). CONISS: a FORTRAN 77 program for stratigraphically constrained cluster analysis by the method of incremental sum of squares. *Comput. Geosci.* 13, 13–35. doi: 10.1016/0098-3004(87)90022-7

Harrison, P. J., Boyd, P. W., Varela, D. E., and Takeda, S. (1999). Comparison of factors controlling phytoplankton productivity in the NE and NW subarctic pacific gyres. *Prog. Pceanogr.* 43, 205–234. doi: 10.1016/S0079-6611(99)00015-4

Hasle, G. R., and Heimdal, B. R. (1968). Morphology and distribution of the marine centric diatom thalassiosira antarctica comber. *J. R. Microscopical Society* 88, 357–369. doi: 10.1111/j.1365-2818.1968.tb00618.x

Haug, G. H., Sigman, D. M., Tiedemann, R., Pedersen, T. F., and Sarnthein, M. (1999). Onset of permanent stratification in the subarctic pacific ocean. *Nature* 401, 779–782. doi: 10.1038/44550

Hemming, S. R. (2004). Heinrich Events: Massive late pleistocene detritus layers of the north Atlantic and their global climate imprint. *Rev. Geophys.* 42, RG1005. doi: 10.1029/2003rg000128

Herguera, J. C., Herbert, T., Kashgarian, M., and Charles, C. (2010). Intermediate and deep water mass distribution in the pacific during the last glacial maximum inferred from oxygen and carbon stable isotopes. *Quaternary Sci. Rev.* 29, 1228–1245. doi: 10.1016/j.quascirev.2010.02.009

Honda, M. C., Imai, K., Nojiri, Y., Hoshi, F., Sugawara, T., and Kusakabe, M. (2002). The biological pump in the northwestern north pacific based on fluxes and major components of particulate matter obtained by sediment-trap experiments, (1997–2000). *Deep Sea Res. Part II: Topical Stud. Oceanography* 49, 5595–5625. doi: 10.1016/S0967-0645(02)00201-1

Honjo, S. (1984). Study of ocean fluxes in time and space by bottom-tethered sediment trap arrays: a recommendation. *Natl. Acad. Press* (Proceedings of a Workshop), 305–324.

Honjo, S., and Doherty, K. W. (1988). Large Aperture time-series sediment traps; design objectives, construction and application. *Deep Sea Res. Part A. Oceanographic Res. Papers.* 35, 133–149. doi: 10.1016/0198-0149(88)90062-3

Hopmans, E. C., Weijers, J. W. H., Schefuß, E., Herfort, L., Sinninghe Damsté, J. S., and Schouten, S. (2004). A novel proxy for terrestrial organic matter in sediments based on branched and isoprenoid tetraether lipids. *Earth Planetary Sci. Lett.* 224, 107–116. doi: 10.1016/j.epsl.2004.05.012

Horner, R., and Alexander, V. (1972). Algal populations in Arctic sea ice: An investigahon of heterotrophy lmnol. *Oceanogr* 17, 454–458. doi: 10.4319/lo.1972.17.3.0454

Hoshiba, M., Ahagon, N., Ohkushi, K., Uchida, M., Motoyama, I., and Nishimura, A. (2006). Foraminiferal oxygen and carbon isotopes during the last

34 kyr off northern Japan, northwestern pacific. *Mar. Micropaleontol.* 61, 196–208. doi: 10.1016/j.marmicro.2006.07.001

Jaccard, S. L., Galbraith, E. D., Sigman, D. M., and Haug, G. H. (2010). A pervasive link between Antarctic ice core and subarctic pacific sediment records over the past 800 kyrs. *Quaternary Sci. Rev.* 29, 206–212. doi: 10.1016/j.quascirev.2009.10.007

Jousé, A. P. (1962). Stratigraphic and paleogeographic investigations in the north-western pacific ocean. *Acad. Sci. USSR*

Katsuki, K., and Takahashi, K. (2005). Diatoms as paleoenvironmental proxies for seasonal productivity, sea-ice and surface circulation in the Bering Sea during the late quaternary. *Deep Sea Res. Part II: Topical Stud. Oceanography* 52, 2110–2130. doi: 10.1016/j.dsr2.2005.07.001

Katsuki, K., Takahashi, K., and Okada, M. (2003). Diatom assemblage and productivity changes during the last 340,000 years in the subarctic pacific. *J. Oceanography* 59, 695–707. doi: 10.1023/B:JOCE.0000009598.93075.78

Keigwin, L. D., Jones, G. A., and Froelich, P. N. (1992). A 15,000 year paleoenvironmental record from meiji seamount, far northwestern pacific. *Earth Planetary Sci. Lett.* 111, 425–440. doi: 10.1016/0012-821X(92)90194-Z

Kim, J., van der Meer, J., Schouten, S., Helmke, P., Willmott, V., Sangiorgi, F., et al. (2010). New indices and calibrations derived from the distribution of crenarchaeal isoprenoid tetraether lipids: Implications for past sea surface temperature reconstructions. *Geochimica Cosmochimica Acta* 74, 4639–4654. doi: 10.1016/j.gca.2010.05.027

Koc Karpuz, N., and Schrader, H. J. P. (1990). Surface sediment diatom distribution and Holocene paleotemperature variations in the Greenland, Iceland and Norwegian Sea. *Paleoceanography Paleoclimatol.* 5, 557–580. doi: 10.1029/PA005i004p00557

Kohfeld, K. E., and Chase, Z. (2011). Controls on deglacial changes in biogenic fluxes in the north pacific ocean. *Quaternary Sci. Rev.* 30, 3350–3363. doi: 10.1016/j.quascirev.2011.08.007

Lam, P. J., Robinson, L. F., Blusztajn, J., Li, C., Cook, M. S., McManus, J. F., et al. (2013). Transient stratification as the cause of the north pacific productivity spike during deglaciation. *Nat. Geosci.* 6, 622–626. doi: 10.1038/ngeo1873

Lembke-jene, L., Tidemann, R., Nürnberg, D., Gong, X., and Lohmann, G. (2018). Rapid shift and millennial-scale variations in Holocene north pacific intermediate water ventilation. *Proc. Natl. Acad. Sci. U. States A.* 115, 5365–5370. doi: 10.1073/pnas.1714754115

Lora, J. M., Mitchell, J. L., and Tripati, A. E. (2016). Abrupt reorganization of north pacific and western north American climate during the last deglaciation. *Geophys. Res. Lett.* 43, 11-796–804. doi: 10.1002/2016gl071244

Maier, E., Méheust, M., Abelmann, A., Gersonde, R., Chapligin, B., Ren, J., et al. (2015). Deglacial subarctic pacific surface water hydrography and nutrient dynamics and links to north Atlantic climate variability and atmospheric CO_2. *Paleoceanography* 30, 949–968. doi: 10.1002/2014pa002763

Marcott, S. A., Bauska, T. K., Buizert, C., Steig, E. J., Rosen, J. L., Cuffey, K. M., et al. (2014). Centennial-scale changes in the global carbon cycle during the last deglaciation. *Nature* 514, 616–619. doi: 10.1038/nature13799

Martin, J. H., and Fitzwater, S. E. (1988). Iron-deficiency limits phytoplankton growth in the northeast pacific subarctic. *Nature* 331, 341–343. doi: 10.1038/331341A0

Matsumoto, K., Oba, T., Lynch-Stieglitz, J., and Yamamoto, H. (2002). Interior hydrography and circulation of the glacial pacific ocean. *Quaternary Sci. Rev.* 21, 1693–1704. doi: 10.1016/S0277-3791(01)00142-1

Max, L., Lembke-Jene, L., Riethdorf, J. R., Tiedemann, R., Nürnberg, D., Kühn, H., et al. (2014). Pulses of enhanced north pacific intermediate water ventilation from the Okhotsk Sea and Bering Sea during the last deglaciation. *Climate Past.* 10, 591–605. doi: 10.5194/cp-10-591-2014

Max, L., Riethdorf, J.-R., Tiedemann, R., Smirnova, M., Lembke-Jene, L., Fahl, K., et al. (2012). Sea Surface temperature variability and sea-ice extent in the subarctic northwest pacific during the past 15,000 years. *Paleoceanography* 27, PA3213. doi: 10.1029/2012pa002292

McManus, J. F., Francois, R., Gherardi, J. M., Keigwin, L. D., and Brown-Leger, S. (2004). Collapse and rapid resumption of Atlantic meridional circulation linked to deglacial climate changes. *Nature* 428, 834–837. doi: 10.1038/nature02494

Méheust, M. (2014). Late quaternary variability of sea-ice cover, surface-water temperature and terrigenous input in the subarctic north pacific and the Bering Sea: A biomarker approach. *PhD Thesis Univ. Bremen.*

Méheust, M., Stein, R., Fahl, K., and Gersonde, R. (2018). Sea-Ice variability in the subarctic north pacific and adjacent Bering Sea during the past 25 ka: New insights from IP_{25} and proxy records. *Arktos* 4, 1–19. doi: 10.1007/s41063-018-0043-1

Méheust, M., Stein, R., Fahl, K., Max, L., and Riethdorf, J.-R. (2015). High-resolution IP_{25}-based reconstruction of sea-ice variability in the western north pacific and Bering Sea during the past 18,000 years. *Geo Marine Lett.* 36, 101–111. doi: 10.1007/s00367-015-0432-4

Mincer, T. J., Church, M. J., Taylor, L. T., Preston, C., Karl, D. M., and DeLong, E. F. (2007). Quantitative distribution of presumptive archaeal and bacterial nitrifiers in Monterey bay and the north pacific subtropical gyre. *Environ. Microbiol.* 9, 1162–1175. doi: 10.1111/j.1462-2920.2007.01239.x

Müller, P. J., Kirst, G., Ruhland, G., Von Storch, I., and Rosell-Melé, A. (1998). Calibration of the alkenone paleotemperature index U37K′ based on core-tops from the eastern south Atlantic and the global ocean (60° n-60° s). *Geochimica Cosmochimica Acta* 62, 1757–1772. doi: 10.1016/S0016-7037(98)00097-0

Naafs, B. D. A., Hefter, J., and Stein, R. (2013). Millennial-scale ice rafting events and Hudson strait heinrich(-like) events during the late pliocene and pleistocene: a review. *Quaternary Sci. Rev.* 80, 1–28. doi: 10.1016/j.quascirev.2013.08.014

Narita, H., Sato, M., Tsunogai, S., Murayama, M., Ikehara, M., Nakatsuka, T., et al. (2002). Biogenic opal indicating less productive northwestern north pacific during the glacial ages. *Geophys. Res. Lett.* 29, 221–224. doi: 10.1029/2001gl014320

NGRIP Dating Group (2006). "Greenland Ice core chronology 2005, (GICC05). IGBP PAGES/World data center for paleoclimatology," in *Data contribution series # 2006-118. NOAA/NCDC paleoclimatology program*(Boulder CO, USA: NOAA/NCDC paleoclimatology program).

Okada, M. (2002). Chemical syntheses of biodegradable polymers. *Prog. Polymer Sci.* 27, 87–133. doi: 10.1016/S0079-6700(01)00039-9

Okazaki, Y., Takahashi, K., Onodera, J., and Honda, M. C. (2005). Temporal and spatial flux changes of radiolarians in the northwestern pacific ocean during 1997–2000. *Deep Sea Res. Part II: Topical Stud. Oceanography* 52, 2240–2274. doi: 10.1016/j.dsr2.2005.07.006

Okazaki, Y., Timmermann, A., Menviel, L., Harada, N., Abe-Ouchi, A., Chikamoto, M. O., et al. (2010). Deepwater formation in the north pacific during the last glacial termination. *Science* 329, 200–204. doi: 10.1126/science.1190612

Onodera, J., and Takahashi, K. (2005). Silicoflagellate fluxes and environmental variations in the northwestern north pacific during December 1997–may 2000. *Deep Sea Res. Part I: Oceanographic Res. Papers.* 52, 371–388. doi: 10.1016/j.dsr.2004.10.001

Otosaka, S., and Noriki, S. (2005). Relationship between composition of settling particles and organic carbon flux in the Western north pacific and the Japan Sea. *J. Oceanography* 61, 25–40. doi: 10.1007/s10872-005-0017-3

Pahnke, K., Goldstein, S. L., and Hemming, S. R. (2008). Abrupt changes in Antarctic intermediate water circulation over the past 25,000 years. *Nat. Geosci.* 1, 870–874. doi: 10.1038/ngeo360

Parrenin, F., Masson-Delmotte, V., Kohler, P., Raynaud, D., Paillard, D., Schwander, J., et al. (2013). Synchronous change of atmospheric CO_2 and Antarctic temperature during the last deglacial warming. *Science* 339, 1060–1063. doi: 10.1126/science.1226368

Poulin, M., Daugbjerg, N., Gradinger, R., Ilyash, L., Ratkova, T., and von Quillfeldt, C. (2010). The pan-Arctic biodiversity of marine pelagic and sea-ice unicellular eukaryotes: A first-attempt assessment. *Mar. Biodiversity* 41, 13–28. doi: 10.1007/s12526-010-0058-8

Praetorius, S. K., Condron, A., Mix, A. C., Walczak, M. H., McKay, J. L., and Du, J. (2020). The role of northeast pacific meltwater events in deglacial climate change. *Sci. Advances* 6, 2915. doi: 10.1126/sciadv.aay2915

Praetorius, S., Rugenstein, M., Persad, G., and Caldeira, K. (2018). Global and Arctic climate sensitivity enhanced by changes in north pacific heat flux. *Nat. Commun.* 9, 3124. doi: 10.1038/s41467-018-05337-8

Qiu, B. (2002). Large-Scale variability in the midlatitude subtropical and subpolar 729 north pacific ocean: Observations and causes. *J. Phys. Oceanography* 32, 353–375. doi: 10.1175/1520-0485(2002)032<0353:LSVITM>2.0.CO;2

Rae, J. W. B., Gray, W. R., Wills, R. C. J., Eisenman, I., Fitzhugh, B., Fotheringham, M., et al. (2020). Overturning circulation, nutrient limitation, and warming in the glacial north pacific. *Sci. Advances* 6, 1654. doi: 10.1126/sciadv.abd1654

Rae, J. W. B., Sarnthein, M., Foster, G. L., Ridgwell, A., Grootes, P. M., and Elliott, T. (2014). Deep water formation in the north pacific and deglacial CO_2 rise. *Paleoceanography* 29, 645–667. doi: 10.1002/2013pa002570

Rasmussen, S. O., Andersen, K. K., Svensson, A. M., Steffensen, J. P., Vinther, B. M., Clausen, H. B., et al. (2006). A new Greenland ice core chronology for the last glacial termination. *J. Geophys. Res.* 111, 1–16. doi: 10.1029/2005jd006079

Reimer, P. J., Bard, E., Bayliss, A., Beck, J. W., and Staff, R. A. (2013). IntCal13 and Marine13 radiocarbon age calibration curves 0-50,000 years cal. BP. *Radiocarbon* 55, 1869–1887. doi: 10.2458/azu_js_rc.55.16947

Rella, S. F., Tada, R., Nagashima, K., Ikehara, M., Itaki, T., Ohkushi, K. I., et al. (2012). Abrupt changes of intermediate water properties on the northeastern slope

of the Bering Sea during the last glacial and deglacial period. *Paleoceanography* 27, PA3203. doi: 10.1029/2011pa002205

Ren, J. (2015). *Late pleistocene paleoceanography of the subarctic pacific derived from the diatom record.* (Universität Bremen, Germany: PhD thesis)

Ren, J., Gersonde, R., Esper, O., and Sancetta, C. (2014). Diatom distributions in northern north pacific surface sediments and their relationship to modern environmental variables. *Palaeogeography Palaeoclimatol. Palaeoecol.* 402, 81–103. doi: 10.1016/j.palaeo.2014.03.008

Riethdorf, J., Max, L., Nürnberg, D., Lembke-Jene, L., and Tiedemann, R. (2013). Deglacial development of (sub) sea surface temperature and salinity in the subarctic northwest pacific: Implications for upper-ocean stratification. *Paleoceanography* 28, 91–104. doi: 10.1002/palo.20014

Sancetta, C. (1979). Oceanography of the north pacific during the last 18,000 years: Evidence from fossil diatoms. *Mar. Micropaleontol.* 4, 103–123. doi: 10.1016/0377-8398(79)90009-4

Sancetta, C. (1982). Distribution of diatom species in surface sediments of the Bering and Okhotsk seas. *Micropaleontology* 28, 221–257. doi: 10.2307/1485181

Sancetta, C. (1992). Comparison of phytoplankton in sediment trap time series and surface sediments along a productivity gradient. *Paleoceanography* 7, 183–194. doi: 10.1029/92PA00156

Sancetta, C., and Calvert, S. E. (1988). The annual cycle of sedimentation in Saanich inlet, British Columbia: Implications for the interpretation of diatom fossil assemblages. *Br. Columbia Deep Sea Res.* 35, 71–90. doi: 10.1016/0198-0149(88)90058-1

Sarnthein, M., Gebhardt, H., Kiefer, T., Kucera, M., Cook, M., and Erlenkeuser, H. (2004). Mid Holocene origin of the sea-surface salinity low in the subarctic north pacific. *Quaternary Sci. Rev.* 23, 2089–2099. doi: 10.1016/j.quascirev.2004.08.008

Sarnthein, M., Kiefer, T., Grootes, P. M., Elderfield, H., and Erlenkeuser, H. (2006). Warmings in the far northwestern pacific promoted pre-Clovis immigration to America during Heinrich event 1. *Geology* 34, 111. doi: 10.1130/g22200.1

Sattarova, V. V., and Artemova, A. V. (2015). Geochemical and micropaleontological character of deep-Sea sediments from the northwestern pacific near the kuril–kamchatka trench. *Deep Sea Res. Part II: Topical Stud. Oceanography* 111, 10–18. doi: 10.1016/j.dsr2.2014.10.030

Schmittner, A., Galbraith, E. D., Hostetler, S. W., Pedersen, T. F., and Zhang, R. (2007). Large Fluctuations of dissolved oxygen in the Indian and pacific oceans during dansgaard-oeschger oscillations caused by variations of north Atlantic deep water subduction. *Paleoceanography* 22, PA3207. doi: 10.1029/2006pa001384

Schmitt, J., Schneider, R., Elsig, J., Leuenberger, D., Lourantou, A., Chappellaz, J., et al. (2012). Carbon isotope constraints on the deglacial CO_2 rise from ice cores. *Science* 336, 711–714. doi: 10.1126/science.1217161

Schouten, S., Hopmans, E.C., Rosell-Melé, A., Pearson, A., Adam, P., Bauersachs, T., et al. (2013). An interlaboratory study of TEX_{86} and BIT analysis of sediments, extracts, and standard mixtures. *Geochem. Geophys. Geosyst.* 14, 5263–5285. doi: 10.1002/2013GC004904

Schouten, S., Hopmans, E. C., Schefuß, E., and Damste, J. S. S. (2002). Distributional variations in marine crenarchaeotal membrane lipids: a new tool for reconstructing ancient sea water temperatures? *Earth Planetary Sci. Lett.* 204, 265–274. doi: 10.1016/S0012-821X(02)00979-2

Seki, O., Kawamura, K., Ikehara, M., Nakatsuka, T., and Oba, T. (2004). Variation of alkenone sea surface temperature in the Sea of Okhotsk over the last 85 kyrs. *Organic Geochem.* 35, 347–354. doi: 10.1016/j.orggeochem.2003.10.011

Serno, S., Winckler, G., Anderson, R. F., Maier, E., Ren, H., Gersonde, R., et al. (2015). Comparing dust flux records from the subarctic north pacific and Greenland: Implications for atmospheric transport to Greenland and for the application of dust as a chronostratigraphic tool. *Paleoceanography* 30, 583–600. doi: 10.1002/2014pa002748

Shcherbina, A. Y., Talley, L. D., and Rudnick, D. L. (2003). Direct observations of north pacific ventilation: brine rejection in the Okhotsk Sea. *Science* 302, 1952–1955. doi: 10.1126/science.1088692

Shiga, K., and Koizumi, I. (1999). Latest quaternary oceanographic changes in the Okhotsk Sea based on diatom records. *Mar. Micropaleontol.* 38, 91–117. doi: 10.1016/S0377-8398(99)00041-9

Sigman, D. M., Fripiat, F., Studer, A. S., Kemeny, P. C., Martínez-García, A., Hain, M. P., et al. (2021). The southern ocean during the ice ages: A review of the Antarctic surface isolation hypothesis, with comparison to the north pacific. *Quaternary Sci. Rev.* 254, 106732. doi: 10.1016/j.quascirev.2020.106732

Sigman, D. M., Hain, M. P., and Haug, G. H. (2010). The polar ocean and glacial cycles in atmospheric CO_2 concentration. *Nature* 466, 47–55. doi: 10.1038/nature09149

Skinner, L. C., Fallon, S., Waelbroeck, C., Michel, E., and Barker, S. (2010). Ventilation of the deep southern ocean and deglacial CO_2 rise. *Science* 328, 1147–1151. doi: 10.1126/science.1183627

Stabeno, P. J., Bond, N. A., Hermann, A. J., Kachel, N. B., Mordy, C. W., and Overland, J. E. (2004). Meteorology and oceanography of the northern gulf of Alaska, cont. *Shelf Res.* 24, 859–897. doi: 10.1016/j.csr.2004.02.007

Stroynowski, Z., Abrantes, F., and Bruno, E. (2017). The response of the Bering Sea gateway during the mid-pleistocene transition. *Palaeogeography Palaeoclimatol. Palaeoecol.* 485, 974–985. doi: 10.1016/j.palaeo.2017.08.023

Takahashi, K. (1986). Seasonal fluxes of pelagic diatoms in the subarctic pacific 1982-1983. *Deep Sea Res. Part A. Oceanographic Res. Papers.* 33, 1225–1251. doi: 10.1016/0198-0149(86)90022-1

Takeda, S., and Tsuda, A. (2005). An *in situ* iron-enrichment experiment in the western subarctic pacific (SEEDS): Introduction and summary. *Prog. Oceanography* 64, 95–109. doi: 10.1016/j.pocean.2005.02.004

Tanimura, Y. (1992). Seasonal changes in flux and species composition of diatoms: sediment trap results from the Northwest pacific, august 1986-November 1988. *Bull. Natl. Sci. Museum Ser. C.* 18, 121–154.

Teraishi, A., Suto, I., Onodera, J., and Takahashi, K. (2016). Diatom, silicoflagellate and ebridian biostratigraphy and paleoceanography in IODP 323 hole U1343E at the Bering slope site. *Deep Sea Res. Part II: Topical Stud. Oceanography* 125, 18–28. doi: 10.1016/j.dsr2.2013.03.026

Thomas, E., Boscolo-Galazzo, F., Balestra, B., Monechi, S., Donner, B., and Röhl, U. (2018). Early Eocene thermal maximum 3: Biotic response at Walvis ridge (SE Atlantic ocean). *Paleoceanography Paleoclimatol.* 33, 862–883. doi: 10.1029/2018pa003375

Toggweiler, J. R. (1999). Variation of atmospheric CO_2 by ventilation of the ocean's deepest water. *Paleoceanography* 14, 571–588. doi: 10.1029/1999pa900033

Toggweiler, J. R., and Lea, D. W. (2010). Temperature differences between the hemispheres and ice age climate variability. *Paleoceanography* 25, PA2212. doi: 10.1029/2009pa001758

Tsoy, I. B., and Wong, C. S. (1999). Diatom fluxes and preservation in the deep northwest pacific ocean. *Proc. 14th Int. Diatom Symposium* 9, 523–549. doi: 10.13140/RG.2.1.4099.6568

Venrick, E. L. (1971). Recurrent groups of diatom species in the north pacific. *Ecology* 52 (4), 614–625. doi: 10.2307/1934149

Venrick, E. L. (1991). Mid-ocean ridges and their influence on the large-scale pattern of chlorophyll and production in the north pacific. *Deep Sea Res.* 38, 83–102. doi: 10.1016/S0198-0149(12)80006-9

Walczak, M. H., Mix, A. C., Cowan, E. A., Fallon, S., Fifield, L. K., Alder, J. R., et al. (2020). Phasing of millennial-scale climate variability in the pacific and Atlantic oceans. *Science* 370, 716–720. doi: 10.1126/science.aba7096

Warren, B. A. (1983). Why is no deep water formed in the north pacific? *J. Mar. Res.* 41, 327–347. doi: 10.1357/002224083788520207

Yao, Z., Liu, Y., Shi, X., Gong, X., Gorbarenko, S. A., Bosin, A. A., et al. (2022). Paleoproductivity variations and implications in the subarctic northwestern pacific since MIS 7: Geochemical evidence. *Global Planetary Change* 209, 103730. doi: 10.1016/j.gloplacha.2021.103730

Yasuda, I. (1997). The origin of the north pacific intermediate water. *J. Geophys. Res Oceans* 102, 893–909. doi: 10.1029/96JC02938

You, Y. (2003). Implications of cabbeling on the formation and transformation mechanism of north pacific intermediate water, J. *Geophys. Res.* 108, 3134. doi: 10.1029/2001JC001285

Zhang, Y. G., and Liu, X. (2018). Export depth of the TEX_{86} signal. *Paleoceanography Paleoclimatol.* 33, 666–671. doi: 10.1029/2018PA003337

Zhong, Y., Liu, Y., Yang, X., Zhang, J., Liu, J., Bosin, A., et al. (2020). Do non-dipole geomagnetic field behaviors persistently exist in the subarctic pacific ocean over the past 140 ka? *Sci. Bull.* 65, 1505–1507. doi: 10.1016/j.scib.2020.05.016